JOURNAL OF Materials CHEMISTRY

Novel modified graphite as anode material for lithium ion batteries

Qinmin Pan, Kunkun Guo, Lingzhi Wang and Shibi Fang*

Institute of Chemistry, Chinese Academy of Sciences, Beijing 100080, P. R. China. E-mail: fangsb@infoc3.icas.ac.cn; Fax: 86+10+62559373; Tel: 86+10+62637541

Received 7th January 2002, Accepted 5th March 2002
First published as an Advance Article on the web 8th April 2002

A novel graphite material for lithium ion batteries was prepared by encapsulation of an ionic conductive polymer on the surface of natural graphite particles *via* radiation-initiated polymerization. The graphite obtained shows great improvement in electrochemical performance such as initial coulombic efficiency and cycleability compared with the original natural graphite. Raman spectroscopy indicates that the structural stability of the graphite surface is enhanced due to the fact that encapsulated polymers can depress the exfoliation of graphite layers caused by co-intercalation of solvent molecules. The solid electrolyte interface (SEI) film formed on the encapsulated graphite electrode retains a stable morphology during repeated cycling, and thus avoids an increase in the electrode's impedance.

Introduction

Much effort has been devoted to the study of natural graphite in the last decade with the aim of using it as the anode material for lithium ion batteries. However, large irreversible capacity loss and poor cycling life have been persistent problems that limit wide application of natural graphite anodes.[1–6] This is due to the fact that natural graphite is a layered material with anisotropic surface structure and that there are weak bonds (van der Waals forces) between the graphene layers.[1–8] These structural characteristics cause two unavoidable problems. (1) Profound differences in chemical and electrochemical reactivity of the basal plane and the edge plane determine the heterogeneity and fragility of the SEI film formed. Numerous studies have shown that composition and morphology of the SEI film on the basal plane and the edge plane were very different. However, the nature of the SEI film plays a significant role in the electrochemical performance of the graphite anode.[3–7] (2) Weak van der Waals forces between graphene layers cannot resist the expansion of the layer spacing and co-intercalation of solvent molecules during the lithium intercalation process. The net result of these problems is that small volume and surface changes of the graphite particle will cause a breakdown of the SEI film formed, and thus repair of the SEI film on a small scale is unavoidable.[1–7] This is the reason for the large irreversible capacity loss and limited cycling life of the graphite anode.

In order to control the irreversible capacity and enhance the cycling life of the natural graphite anode, Aubach *et al*. have concluded that it is necessary to make the SEI film formed very compact and flexible.[8–10] So that the SEI film can accommodate the volume and surface changes of graphite particles during cycling, and thus minimize the side reactions such as co-intercalation of solvent molecules, attention has been paid to the modification of the electrode/electrolyte interface of the graphite electrode which has previously proved to be an effective way of improving the electrochemical performance of the graphite anode.[11–15] However, the SEI film formed on these graphite electrodes is still believed to lack elasticity and flexibility.

The interests of our group has been focused on the surface encapsulation of natural graphite particles with ionic conductive polymers. The aim of our work has been to form ionic conductive polymer films on the surface of graphite particles which are compact and sufficiently flexible to prevent co-intercalation of the solvated Li ion, thus reducing irreversible capacity and enhancing cycleability. Of course, the encapsulated polymer film should have sufficient ionic conductivity to permit reversible intercalation/de-intercalation of Li ion at suitable rates. To achieve these goals, a radiation-initiated polymerization technique was used to prepare the ionic conductive polymer encapsulated graphite material. The advantage of this method is that it usually provides good homogeneity and the film is easy to produce. In our previous work,[16] we reported excellent electrochemical properties of poly(lithium styrenesulfonate) (PSSALi) encapsulated graphite as the anode material for lithium ion batteries. To further investigate the effect of encapsulation of ionic conductive polymer on graphite on the lithium intercalation/de-intercalation properties of natural graphite, poly(methacrylate hexylsufonic acid) lithium salt†(poly(MHSALi)) was encapsulated on a natural graphite surface and its electrochemical properties were comprehensively studied.

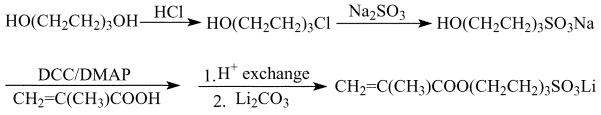

Scheme 1

Experimental

The natural graphite powder used in this study was obtained from Nanshu Graphite Co. (Shandong province, P. R. China) and was labeled as N-graphite. The mean particle size and the Brunauer–Emmett–Teller (BET) surface area of the N-graphite were 17.6 μm and 12.4 m^2g^{-1}, respectively. Scanning electron microscopy (SEM, S-530, Hitachi) was employed to investigate the surface morphology of the N-graphite.

The mechanism for the synthesis of poly(methacrylate hexylsufonic acid) lithium salt [poly(MHSALi)] is shown as follows (Scheme 1), where DCC and DMAP are *N*,*N*′-dicyclohexylcarbodiimide and 4-dimethylaminopyridine, respectively.

Elemental analysis, calculated for $C_{10}H_{17}O_5SLi$: C, 46.88%; H, 6.64%; O, 31.25%; S, 12.52%; found: C, 47.03%; H, 6.78%; S, 12.41%, O, 31.46%.

Polymerization of methacrylate hexylsufonic acid lithium

†The IUPAC name for methacrylate hexylsulfonic acid lithium salt is lithium sulfonatohexyl methacrylate.

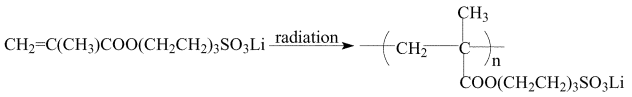

Scheme 2

salt (MHSALi) was conducted using a cobalt 60 γ-ray source in a radiation tube as described in the following procedure (Scheme 2). Natural graphite powder and a given amount of MHSALi monomer (9 : 1.3, by weight) were added to dry methanol and vigorously stirred. The mixture was then transferred to a radiation tube filled with N_2 and held under a cobalt 60 γ-ray source, and polymerization was allowed to take place until a radiation dose of 4 million rad had been reached. After reaction, the mixture was filtered and no free monomers were detected, the resultant graphite was rinsed with methanol and dried. The graphite powder obtained was called encapsulated graphite (E-graphite).

FT-IR spectra were obtained on a Perkin-Elmer apparatus (FT-IR Spectrometer 1000) using the KBr disc method.

XPS (X-ray photoelectron spectroscopy, ESCALAB2020I-XL) measurements were performed in a ultrahigh vacuum (UHV) (2.5×10^{-10} Torr base pressure) with the use of a monochromatic Al-Kα source (1486.6 eV). The depth profiles were obtained by argon-ion sputtering (4 kV) at a sputtering rate of 20 Å min^{-1} on a SiO_2–Si sample to determine the thickness of the encapsulated polymer film.

To produce Raman spectra the encapsulated graphite was excited using radiation with a wavelength of 514.5 nm (50 mW) from an argon ion laser (NEC, GLG3260). The Raman spectra were then recorded using a Raman spectrometer (Jobin-Yvon T-64000) equipped with a multichannel charge-coupled device (CCD) detector.

Preparation of graphite electrodes and the assembly of cells was described elsewhere.[1–4] The electrolyte used was 1 mol L^{-1} $LiPF_6$ solution in a 1 : 1 : 1 (by volume) mixture of ethylene carbonate (EC), diethylene carbonate (DEC) and propylene carbonate (PC). The cells were discharged and charged between 0.010 and 2.000 V *vs.* Li/Li^+ at a constant current of 0.25 mA cm^{-2} using a computer-controlled battery tester. Cyclic voltammograms (CV) were obtained using a three electrode cell at a scan rate of 0.2 mV s^{-1}.

Electrochemical impedance measurements were carried out using an IM6e impedance analyzer (Zahner Electrik). Impedance spectra were potentiostatically measured by applying an a.c. voltage of 5 mV amplitude over the frequency range 10 kHz to 10 mHz after the electrode had attained an equilibrium at each potential. All the potentials indicated here are referenced to the Li/Li^+ electrode potential.

After cycling, the cycled cells were transferred to a glove box filled with argon and graphite foils were peeled from the copper collector. Then the graphite foils were immersed into diethyl carbonate (DEC) solvent to remove soluble species for 1 week and dried in the glove box. Scanning electron microscopy (SEM, S-530, Hitachi) was used to investigate the morphology of the SEI films formed.

Results and discussion

1. Characterization of the encapsulated graphite

Fig. 1 shows the scanning electron microscopic images of the natural graphite (N-graphite) and poly(MHSALi) encapsulated graphite (E-graphite) samples. These images show very clearly that the N-graphite surface displays aligned graphite flakes with distinct edge planes, whereas the surface of E-graphite particles shows different morphology, the distinct edge planes have disappeared and the particles are apparently covered by a thin film.

Fig. 2 displays the FT-IR spectra of the natural and encapsulated graphite samples. Obviously, no peak corresponding to

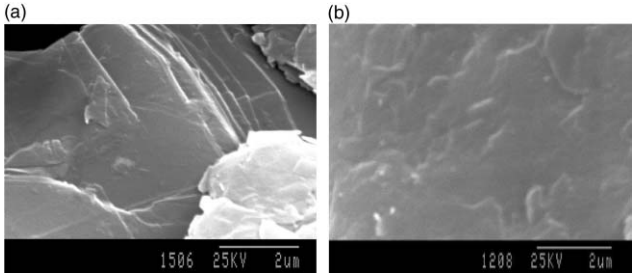

Fig. 1 Scanning electron microscope images of the natural graphite sample before and after encapsulation of poly(MHSALi): (a) natural graphite, (b) encapsulated graphite.

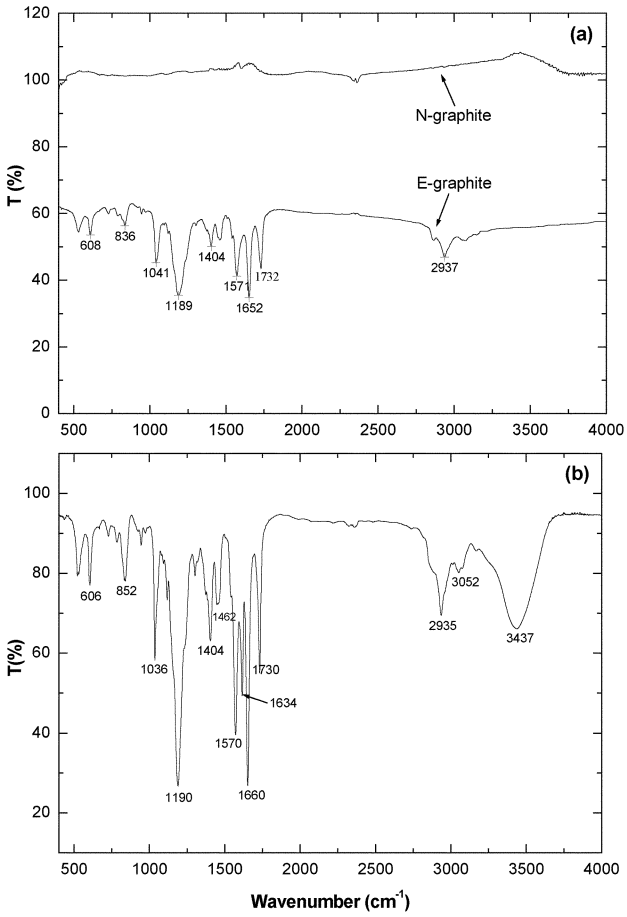

Fig. 2 FT-IR spectra of the N-graphite, E-graphite and monomer: (a) N-graphite and E-graphite, (b) monomer.

the specific bond vibration of C=C (1634 cm^{-1}) in the monomers is found on the surface of E-graphite. However Fig. 2 does show that the specific vibration peaks ascribed to poly(MHSALi) that appear after radiation are SO_3 (1404 cm^{-1}) and O–C=O (1732 cm^{-1}, 1651 cm^{-1}, 1571 cm^{-1}, 1040 cm^{-1}).

Fig. 3 shows the XPS profiles of the encapsulated graphite sample before and after 30 min of argon ion sputtering at a rate of 20 Å min^{-1}. Clearly, the C_{1s} peaks for C–C in the polymer (284.6 eV), O–C=O (288.3 eV) and C–S (285.9 eV), S_{2p} for SO_3 (168.1 eV), O_{1s} for S=O (531.38 eV), S–O (535.7 eV) and O–C=O (532.8 eV), and Li_{1s} for SO_3Li (62.58 eV), which is assigned to the polymer, are observed at 0 min. After 30 minutes etching, the N_{1s}, S_{2p} and Li_{1s} peaks relating to the polymer disappear and the C_{1s} peak (284.6 eV), assigned to the natural graphite, appears.[17–19] The SEM images, FT-IR and XPS spectra demonstrate that the surface of the E-graphite is coated with poly(MHSALi) film with a thickness of about 60 nm.

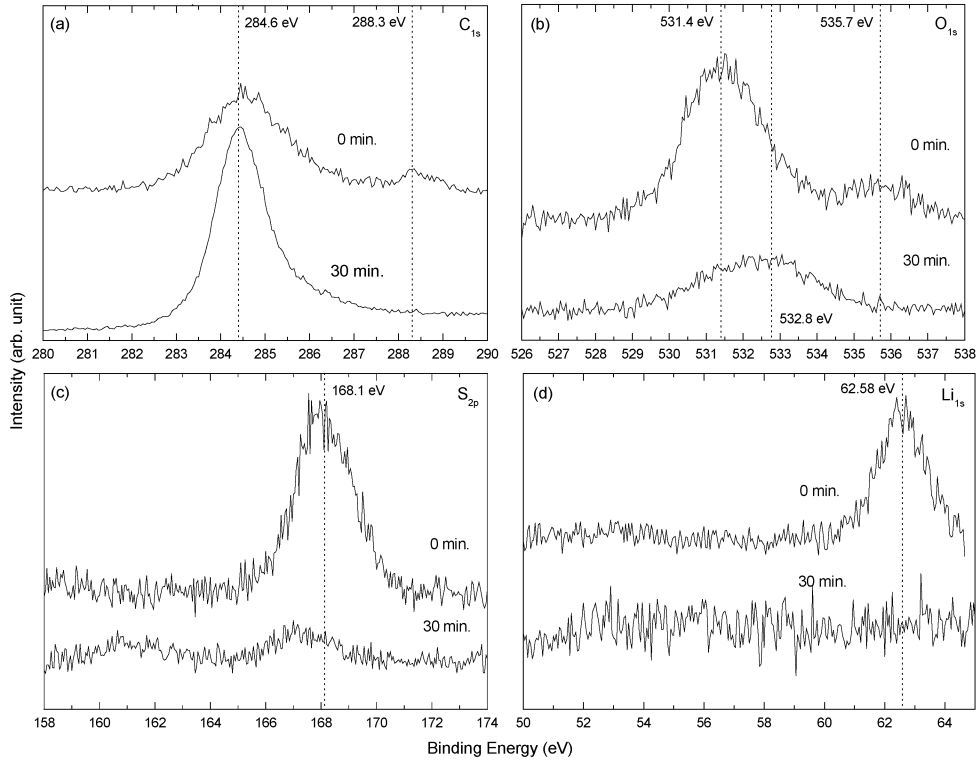

Fig. 3 X-Ray photoelectron spectra for carbon C_{1s}, oxygen O_{1s}, sulfur S_{2p} and lithium Li_{1s} in the encapsulated graphite samples before and after 30 min sputtering, sputtering rate 20 Å min^{-1}: (a) C_{1s}, (b) O_{1s}, (c) S_{2p}, (d) Li_{1s}.

2. Discharge–charge properties of the encapsulated graphite

Fig. 4 shows the first discharge–charge (intercalation/de-intercalation) profiles of the N-graphite and E-graphite electrodes. A plateau at about 0.75 V in the discharge curve was observed for the N-graphite electrode (see Fig. 4a); this plateau is ascribed to electrolyte decomposition and SEI film formation.[2,3] Clearly this plateau is much smaller for the E-graphite electrode (see Fig. 4b). Accordingly, the irreversible capacity consumed on formation of SEI film on the E-graphite electrode is expected to be lower and the initial coulombic efficiency is enhanced (from 70.1% to 85.5%).

The cyclic voltammograms (CV) of the N-graphite and E-graphite electrodes are illustrated in Fig. 5. Two cathodic (reduction) peaks in the potential range of 0.6–0.9 V and 0.3–0.6 V are observed for N-graphite in the first cycle, and these peaks disappear during the second cycle [see Fig. 5a]. These peaks are associated with the SEI film formation (0.6–0.9 V) and co-intercalation of solvated Li^+ (0.3–0.6 V), respectively.[13,14] Evidently, the peak relating to co-intercalation of solvated Li^+ is larger than the peak due to SEI film formation, which implies that co-intercalation of solvated Li^+ contributes mostly to the irreversible capacity loss of the N-graphite electrode. However, these peaks decrease dramatically after encapsulation by poly(MHSALi) [see Fig. 5b], and there is no difference in the anodic peaks (de-intercalation process) between the two graphite electrodes. These results indicate that encapsulation of poly(MHSALi) film on the natural graphite surface can depress the irreversible capacity caused by formation of the SEI film and co-intercalation of solvated Li^+, but it has no effect on the lithium de-intercalation process.

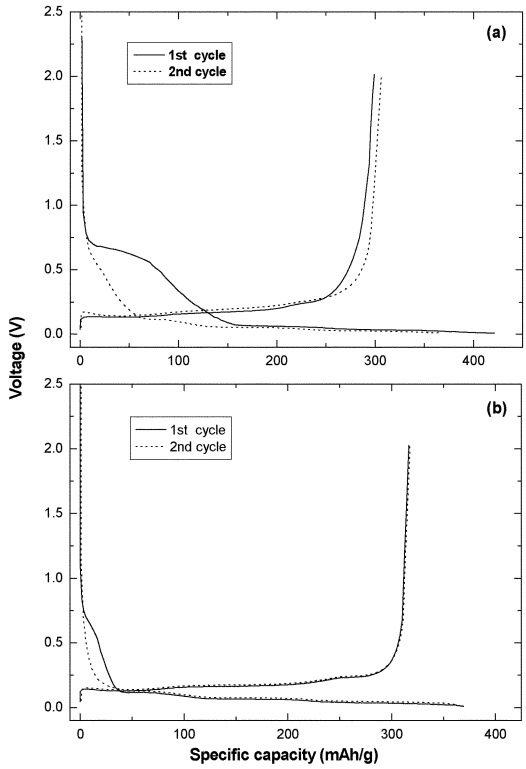

Fig. 4 Discharge–charge profiles of the natural and encapsulated graphite electrodes in PC-based electrolyte: (a) natural graphite, (b) encapsulated graphite.

3. Raman spectroscopy study

As has been reported previously,[8–10] co-intercalation of solvated Li^+ in natural graphite electrodes leads to exfoliation of the graphene layers and consequent amorphization of the graphite surface; Raman spectra is proven to be an effective method with which to investigate the surface changes of graphite electrodes. Fig. 6 displays Raman spectra of two graphite electrodes before and after the first discharge–charge cycle. As seen in Fig. 6, compared to the original N-graphite, an E_{2g} band with a weak shoulder at 1580 cm^{-1} is observed for

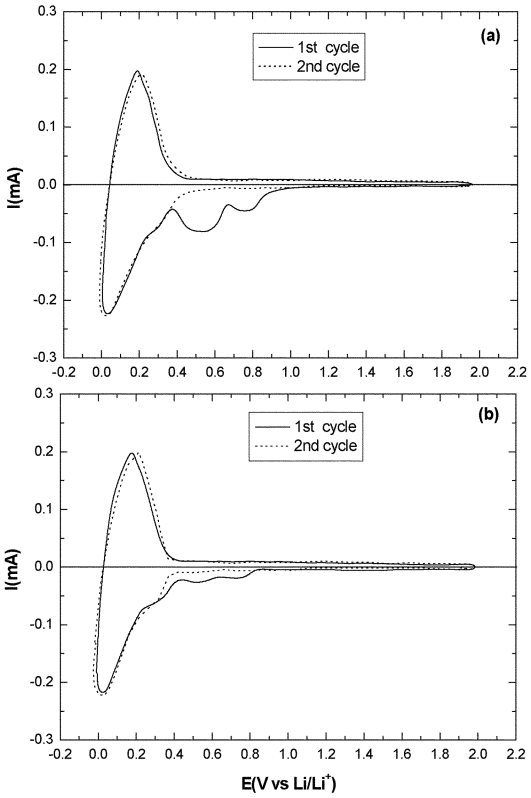

Fig. 5 Cyclic voltammograms of natural and encapsulated graphite electrodes in PC-based electrolyte: (a) natural graphite, (b) encapsulated graphite.

the N-graphite electrode after the first lithium de-intercalation process (see Fig. 6a), which suggests that the top layers of the N-graphite surface were somewhat damaged during the first

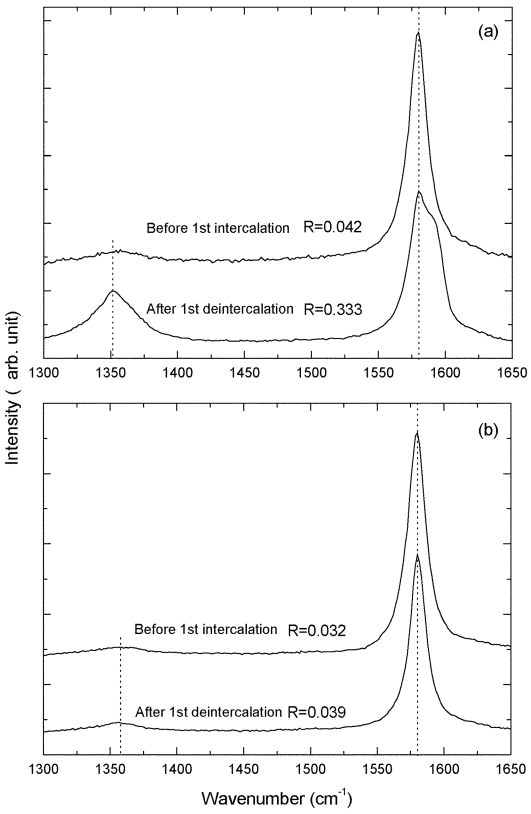

Fig. 6 Raman spectra of the natural and encapsulated graphite electrodes before and after the first cycle, (a) natural graphite electrode: (b) encapsulated graphite electrode.

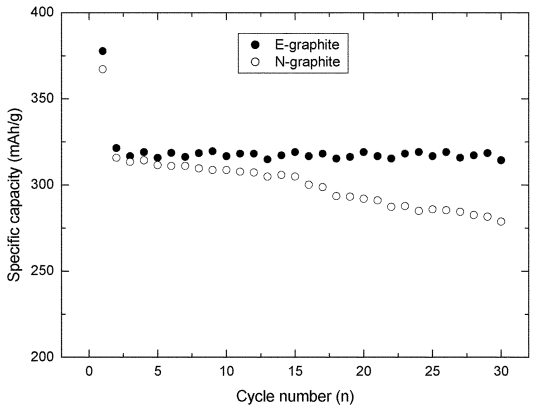

Fig. 7 Cycling characteristics of the natural and encapsulated graphite electrodes in PC-based electrolyte.

cycle and could not be returned to the original graphite structure.[20–22] In contrast, the E_{2g} bands of the E-graphite electrode exhibit no change in peak intensity or in bandwidth before intercalation and after de-intercalation (see Fig. 6b). This conclusion is also supported by the appearance of the peak at 1352 cm^{-1} and variation of the R (the ratio of peak intensity at 1352 cm^{-1} to that at 1580 cm^{-1}, *i.e.* I_{1352}/I_{1580}) value in Fig. 6. It was accepted that the peak at around 1352 cm^{-1} (A_{1g} mode) is generally considered to originate from some kind of imperfection and disorder such as defects, discontinuity in crystallites, and stacking disorder in the crystal structure of graphite, and the R-value indicates the ratio of graphite edge planes and/or the boundary of the graphite plane.[20–23] The R-value of the N-graphite electrode increases rapidly from 0.042 to 0.333, while a stable value (from 0.032 to 0.039) is typical of the E-graphite electrode. The increase in the R-value and the appearance of a band at 1352 cm^{-1} indicate decreasing crystallite size of the N-graphite and increasing imperfection

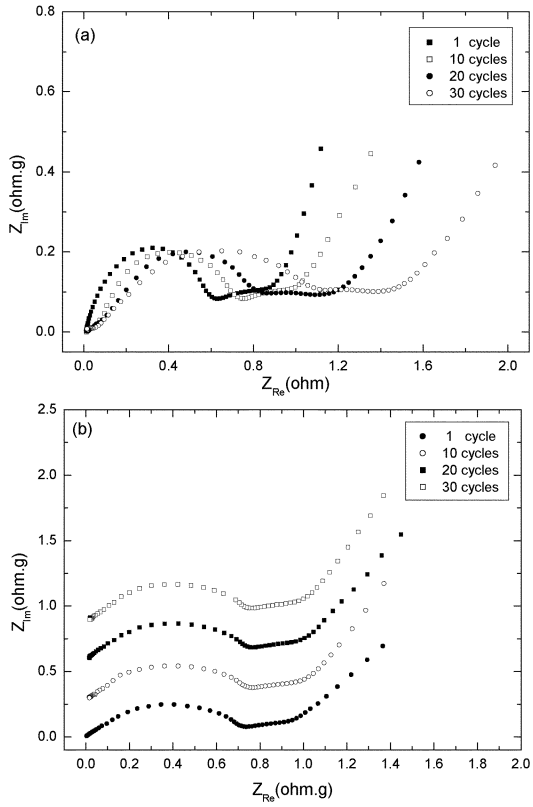

Fig. 8 Electrochemical impedance spectra of the natural and encapsulated graphite electrodes after difference cycling numbers: (a) natural graphite, (b) encapsulated graphite.

and disorder in the crystal structure after cycling. We can reasonably ascribe this damage to an effect of the exfoliation process. The Raman spectra imply that as a result of encapsulation of poly(MHSALi) on N-graphite the graphite surface can resist destruction during the Li intercalation process, which verifies further that encapsulation of poly-(MHSALi) can depress the co-intercalation of solvated Li^+.

4. Cycling characteristics of the encapsulated graphite

Discharge–charge cycling behavior of the E-graphite and N-graphite electrodes in PC-based electrolyte are presented in Fig. 7. The E-graphite electrode shows stable capacity and lower capacity loss compared with that of the N-graphite upon prolonged cycling. Overall, the E-graphite electrode reveals higher reversible capacity and better cycleability than that of the N-graphite.

Fig. 8 shows the impedance spectra of the E-graphite and N-graphite electrodes after different cycling numbers. Two depressed semicircles in high and middle frequency regions are observed for both electrodes as seen in Fig. 8. As has been reported previously,[24–28] the semicircle in high-frequency regions is due to Li ion migration through the SEI film, whereas the semicircle in middle-frequency region corresponds to the charge-transfer reaction at the interface between graphite and the SEI film. Upon cycling, the semicircles (in both the high and middle frequency region) of the N-graphite electrode enlarged appreciably (see Fig. 8a), while the semicircle size of the E-graphite electrode remains almost unchanged (see Fig. 8b). Enlargement of the semicircle in the high-frequency region suggests thickening of the SEI film after cycling. Meanwhile, increasing the charge-transfer resistance of the N-graphite electrode also indicates that the SEI film is increasingly detrimental to the reversible intercalation/de-intercalation of lithium ions during the cycling process. This can be explained by the fact that exfoliation of the graphene layers induced by the co-intercalation of solvent molecules leads to a breakdown of the SEI film, and thus to continuous reduction of electrolyte components and growth of the SEI film on a small scale.[9,10] Therefore, one mechanism for capacity loss of the N-graphite electrode is considered to be the pronounced increase in its impedance during repeated cycling leading to electrical disconnection of the graphite particles. In contrast, additional growth of the SEI film on the E-graphite electrode is

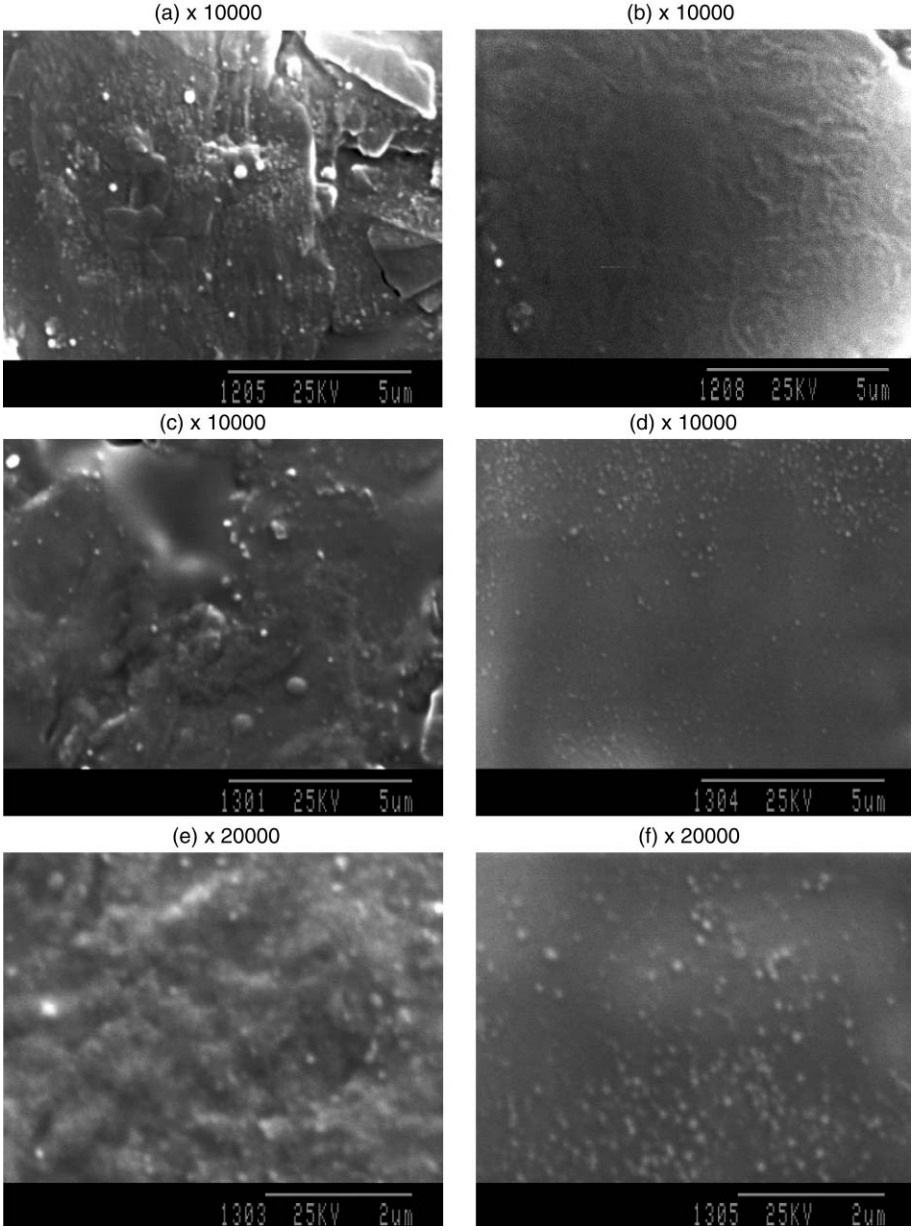

Fig. 9 SEM images of the SEI film formed on natural and encapsulated graphite: (a) N-graphite, 1 cycle, (b) E-graphite, 1 cycle, (c, e) N-graphite, 30 cycles, (d, f) E-graphite, 30 cycles.

avoided, thus maintaining constant electrochemical kinetics during the cycling, as reflected in Fig. 8b.

5. Morphology of SEI film on the graphite surface

The good cycleability of the E-graphite can also be explained by the morphology of the SEI film formed, as seen from the SEM images in Fig. 9; after 1 cycle the SEI film of the N-graphite consists of small particles whose diameters are on the nanoscale; the particles are evenly distributed on the graphite surface. In contrast, the morphology of the SEI film on the E-graphite is shown to be a compact, consolidated and thin film which means that the encapsulated polymer can act as the SEI film formed *via* electrochemical decomposition. After 30 cycles, the surface of the N-graphite electrode becomes rougher and the particles grow larger, and the porosity of the surface is increased. The SEM images of the N-graphite electrode demonstrate that additional growth and thickening of the SEI film during cycling is unavoidable in the PC containing electrolyte.[28–30] In contrast, the SEI film formed on the E-graphite electrode is shown still to be a compact and homogeneous film after 30 cycles. It should be noted that a few nanoparticles appear on the surface of the E-graphite after repeated cycling. This implies that additional growth of the SEI film still takes place on a very small scale even for encapsulated graphite.

We attribute the high cycling stability of the E-graphite electrodes (of both their capacity and impedance upon cycling) to the stability of their SEI film. As discussed above, the SEI film formed on the E-graphite contains an elastic component and is more flexible and protective, which can better accommodate the volume and surface changes of the graphite electrode during repeated cycling.[8–10] As a result, the additional growth of the SEI film common to natural graphite electrodes in the PC-based electrolyte can be avoided, and the morphology of the SEI film formed on the E-graphite electrode and its impedance remain unchanged during the cycling.

Conclusion

The results of this study demonstrate that encapsulation of an ionic conductive polymer poly(MHSALi) on the surface of natural graphite cannot only depress the irreversible capacity due to co-intercalation of solvated Li^+ and exfoliation of the graphite layers, but also avoid a pronounced increase in an electrode's impedance. Encapsulation of poly(MHSALi) contributes to the stability and elasticity of the SEI film formed and thus can accommodate volume and surface changes of the graphite particles during cycling. As a result, the encapsulated graphite electrodes show great improvement in the initial coulombic efficiency and cycleability in PC-based electrolyte compared to that of natural graphite. Overall, encapsulation of an ionic conductive polymer on natural graphite is proven to be a promising approach for reducing the irreversible capacity and improving the cycleability.

Acknowledgement

The authors would like to thank Dr Yongfang Li for his discussion and support during this research. The authors also wish to express their gratitude to the Natural Sciences Fund of China (50173029), with regard to its financial support.

References

1 P. Arora and R. E. White, *J Electrochem. Soc.*, 1998, **145**, 3647.
2 K. Tatsumi, N. Iwashita, H. Sakaebe and H. Shioyama, *J. Electrochem. Soc.*, 1995, **142**, 716.
3 G. C. Chung, S. H. Jun, K. Y. Lee and M. H. Kim, *J. Electrochem. Soc.*, 1999, **146**, 1664.
4 K. Suzuki, T. Hamada and T. Sugiura, *J. Electrochem. Soc.*, 1999, **146**, 890.
5 G. C. Chung, H. J. Kim, S. H. Yu and S. H. Jun, *J. Electrochem. Soc.*, 2000, **147**, 4391.
6 H. Shi, J. Barker, M. Y. Saidi and R. Koksbang, *J. Electrochem. Soc.*, 1996, **143**, 3466.
7 J. S. Gnanaraj, M. D. Levi, E. Levi, G. Salitra and D. Aurbach, *J. Electrochem. Soc.*, 2001, **148**, A525.
8 D. Aurbach, B. Matkovsky, I. Weissman, E. Levi and Y. Ein-Eli, *Electrochim Acta*, 1999, **45**, 67.
9 D. Aurbach, B. Markovsky, M. D. Levi, E. Levi and A. Schechter, *J. Power Sources*, 1999, **81-82**, 95.
10 D. Aurbach, *J. Power Sources*, 2000, **89**, 206.
11 E. Peled, C. Menachem, D. Bar-Tow and A. Melman, *J. Electrochem. Soc.*, 1996, **143**, L4.
12 Y. P. Wu, C. Y. Jiang, C. R. Wan and E. Tsuchida, *Electrochem. Commun.*, 2000, **2**, 626.
13 P. Yu, B. S. Haran, J. A. Ritter, R. E. White and B. N. Popov, *J. Power Sources*, 2000, **91**, 107.
14 M. Yoshio, H. Y. Wand, K. Fukuda, Y. Hara and Y. Adachi, *J. Electrochem. Soc.*, 2000, **147**, 1245.
15 T. Tsumura, A. Katanosaka, I. Souma and T. Ono, *Solid State Ionics*, 2000, **135**, 209.
16 Q. M. Pan and S. B. Fang, *Polymer For Advanced Technologies*, in press.
17 D. Bar-Tow, E. Peled and L. Burstein, *J. Electrochem. Soc.*, 1999, **146**, 824.
18 T. Sotomura, K. Adachi, M. Taguchi and M. Iwaku, *J.Power Sources*, 1999, **81-82**, 192.
19 H. Momose, H. Honbo, S. Takeuchi, K. Nishimura and T. Horiba, *J. Power Sources*, 1997, **68**, 208.
20 M. Inaba, H. Yoshida, Z. Ogumi and T. Abe, *J. Electrochem. Soc.*, 1995, **142**, 20.
21 M. Nakamizo and K. Tamai, *Carbon*, 1984, **22**, 197.
22 R. Bowling, R. Packard and R. L. Mccreery, *J. Am. Chem. Soc.*, 1989, **111**, 1217.
23 F. Tuinstra and J. L. Koenig, *J. Chem. Phys.*, 1970, **53**, 1126.
24 E. Barsoukov, J. H. Kim, J. H. Kim, C. O. Yoon and H. Lee, *Solid State Ionics*, 1999, **116**, 249.
25 Y. C. Chang and H. J. Sohn, *J. Electrochem. Soc.*, 2000, **147**, 50.
26 T. Piao, S. M. Park, C. H. Doh and S. I. Moon, *J. Electrochem. Soc.*, 1999, **146**, 2794.
27 M. C. Smart, B. V. Ratnakumar, S. Surampudi and Y. Wang, *J. Electrochem. Soc.*, 1999, **146**, 3963.
28 Funabiki, M. Inaba, Z. Ogumi and S. Yuasa, *J. Electrochem. Soc.*, 1998, **145**, 172.
29 F. Kong, R. Kostecki, G. Nadeau, X. Song and K. Zaghib, *J. Power Sources*, 2001, **97-98**, 58.
30 E. Peled, D. Bar-Tow, A. Merson, A. Gladkich and L. Burstein, *J. Power Sources*, 2001, **97-98**, 52.